SAND2021-12501J

COMMUNICATION

Experimental observation of hydrocarbon growth by resonance stabilized radical-radical chain reaction

David E. Couch[a], Angie J. Zhang[a], Craig A. Taatjes[a], Nils Hansen*[a]

[a] D. E. Couch, A. J. Zhang, C. A. Taatjes, N. Hansen
Gas Phase Chemical Physics Department
Combustion Research Facility
Sandia National Laboratories
Livermore, CA 94550 (USA)
E-mail: nhansen@sandia.gov

Supporting information for this article is given via a link at the end of the document.

Abstract: *Rapid molecular weight growth of hydrocarbons occurs in flames, in industrial synthesis, and potentially in cold astrochemical environments. A variety of high- and low-temperature chemical mechanisms have been proposed and confirmed, but more facile pathways may be needed to explain observations. We provide laboratory confirmation in a controlled pyrolysis environment of a recently proposed mechanism, radical-radical chain reactions of resonance-stabilized species. The recombination reaction of phenyl (c-C_6H_5) and benzyl (c-$C_6H_5CH_2$) radicals produces both diphenylmethane and diphenylmethyl radicals, the concentration of the latter increasing with rising temperature. A second phenyl addition to the product radical forms both triphenylmethane and triphenylmethyl radicals, confirming the propagation of radical-radical chain reactions under the experimental conditions of high temperature (1100-1600 K) and low pressure (~3 kPa). Similar chain reactions may contribute to particle growth in flames, the interstellar medium, and industrial reactors.*

Hydrocarbon molecular weight growth has been the focus of substantial research efforts because of its rich fundamental physical chemistry and its importance in areas from combustion and industrial processing to astrochemistry. Incomplete combustion produces particulate matter composed of polycyclic aromatic hydrocarbons (PAHs), which causes a wide range of human health problems.[1] Industrially, controlled hydrocarbon growth using pyrolysis has emerged as a promising method for economical, high-throughput, low-waste production of high-demand carbon nanomaterials such as nanotubes.[2] Better understanding of elementary growth pathways could open new opportunities for producing nanoparticles and specialized materials.[1b, 3] In addition to these high-temperature pyrolysis environments, an unexplained abundance of PAHs in the low-temperature interstellar medium (ISM)[4] has led to a search in the physical chemistry community[5] for barrierless radical-driven PAH growth mechanisms.

Despite the dramatically different pressure and temperature conditions, similar chemical mechanisms contribute to hydrocarbon growth in both astrochemical and combustion environments. Current understanding describes a bottom-up molecular mass growth process based on various laboratory-confirmed radical-molecule and radical-radical reaction networks. The HACA (hydrogen-abstraction-C_2H_2-addition) mechanism[6] is widely employed to describe hydrocarbon molecular weight growth in combustion[1b] and to a lesser extent in astrochemistry.[4-5, 7] In addition to HACA, the PAC (phenyl-addition-dehydrocyclization) mechanism[8] provides a pathway for addition of multiple rings in a single step, and methyl addition pathways[9] can help explain the prevalence of odd-carbon PAHs. For low temperature environments, the HAVA (hydrogen-abstraction-vinylacetylene-addition) mechanism[7, 10] involves barrierless addition of vinylacetylene and 1,3-butadiene to PAH radicals, and the MACA (methylidyne-addition–cyclization–aromatization) mechanism[11] describes barrierless methylidyne addition to stable PAHs. However, observations of soot formation in flames and high molecular weight species in the ISM may still not be fully explained by these mechanisms.

Radical-radical chain reactions provide a route to rapid hydrocarbon growth in both low- and high-temperature environments in a mechanism termed CHRCR (clustering of hydrocarbons by radical chain reactions).[12] In part of the proposed mechanism, PAHs form without depletion of the radical pool through chain reactions in which radical-radical recombination is followed by an immediate H-atom ejection to form a new resonance-stabilized radical, typically a partially delocalized π-radical with extended conjugation. While most PAH growth mechanisms involve the formation and reactivation of stabilomers (highly stable PAHs), the prompt H loss in CHRCR allows sequential growth without requiring reactivation by H-abstraction or H-addition reactions.

Radical chain reactions provide a promising route to form PAHs in low-temperature astrochemical environments. PAHs account for about 10% of the total interstellar carbon, but their chemical lifetime in that environment is ~20x shorter than the timescale for PAH injection into the ISM from stars.[4] Thus, PAHs likely form directly in the ISM,[4] but few low-temperature growth pathways are known. Furthermore, PAH growth in stellar ejecta may also be driven by low-temperature pathways, as the HACA mechanism seems to require PAHs to pass through a critical temperature region in the circumstellar envelopes of asymptotic giant branch stars many, many times to explain observed PAH ejection.[13] Electronic structure calculations and molecular beam studies have provided insight into low-temperature growth pathways,[5] primarily based on the HAVA[7, 10] and MACA[11] mechanisms which involve specific feedstocks (vinylacetylene, 1,3-butadiene, and methylidyne). Barrierless radical-radical chain reactions provide another low-temperature pathway for PAH formation that does not require repeated H-abstraction. In a nearly collision-free environment, the chain reaction will generally propagate to form a new radical whenever the total recombination/H-loss reaction is exothermic (so the cold reactants have enough energy to complete the dissociation), a requirement satisfied according to

calculations for several recombination reactions.[14] Radical feedstocks can be produced from collisions of carbonaceous ice grains, destruction of PAHs by cosmic radiation, and electron—ion dissociative recombination.

Soot nucleation in flames is extremely challenging to model on a fundamental basis, and chain reactions may contribute to the formation of nucleation initiators. Although low concentrations of radicals in flames could reduce the importance of radical-radical reactions,[15] some combined experimental and modelling studies have found that these reactions contribute substantially to PAH growth.[16] A recent theoretical study on the role of radical-radical recombination in nucleation[17] found that σ-π and π-π recombinations were most promising for initiating nucleation, though calculated elementary rate coefficients for few-ring species were still too low to fully explain nucleation in flames. The CHRCR mechanism[12] suggests a cascade of (mostly σ-π) recombinations followed by H loss to produce a large π-radical "initiator" that begins nucleation. This nearly direct pathway to nucleation from single and double ring aromatics is consistent with the observation of higher concentrations of particulates than of 3-ring and larger PAHs in flames.[18] Several theoretical studies have investigated the possibility of these radical-radical chain reactions, finding in some cases high radical + H yields at high temperatures[14b-d, 19] though not for all radical-radical recombinations.[14a, 14d]

Individual recombination reaction steps can be studied in a flash pyrolysis microreactor. These devices, long used as clean sources of radicals,[20] rapidly heat a controlled mixture of precursors before cooling by expansion into vacuum. In addition to a wide variety of unimolecular decompositions and radical-molecule reactions, several radical-radical recombination reactions have been studied using flash pyrolysis. The self-reactions of phenylpropargyl,[21] phenyl,[22] propargyl,[23] and benzyl[24] radicals, probed using IR/UV dip spectroscopy, produce a variety of closed-shell PAHs including multiple appearances of indene, naphthalene, phenanthrene, and *para*-terphenyl. The self-reaction of propargyl (C_3H_3) radicals was later confirmed to produce benzyne and several benzene isomers using tunable vacuum-ultraviolet light coupled with mass spectrometry.[25] Another study found that methyl addition to indenyl radicals produces naphthalene as well as a very small amount of the methylindenyl radical.[26] In this work, we use a similar flash pyrolysis microreactor to study a radical-radical chain reaction (phenyl + benzyl) in which the first product is a resonance-stabilized radical (diphenylmethyl) that survives the high temperatures to directly contribute to further growth (triphenylmethyl). Both radical reactants, phenyl[27] and benzyl,[16a] have been observed and quantified in certain flames previously, and other σ and π radicals could potentially replace phenyl and benzyl, respectively, in similar radical chain reactions.

The phenyl radical (Ph) + benzyl radical ($PhCH_2$) reaction studied in this work is a good candidate for a chain reaction because the closed-shell adduct, diphenylmethane (Ph_2CH_2), has a sp^3-hybridized carbon that prevents full conjugation. As shown in Scheme 1, following the initial adduct formation, the loss of an H atom forms a diphenylmethyl radical (Ph_2CH) that is best described as a fully conjugated, resonantly stabilized π-radical, exactly the extension of conjugation suggested as a driving force for CHRCR.[12] Matsugi and Miyoshi[14d] explored this reaction theoretically and found that at low pressures (10 Torr) and temperatures above 1500 K, Ph_2CH formation dominates over production of the closed-shell Ph_2CH_2 in a well-skipping reaction where the Ph_2CH_2 potential energy well is "skipped." Though not included in the calculation, subsequent phenyl addition to the Ph_2CH radical (Scheme 1) also produces either an sp^3-hybridized adduct, Ph_3CH, or a conjugated radical, Ph_3C, both of which are observed here. The Ph addition could also occur at the *ortho* or *para* sites of $PhCH_2$, and these isomers are also likely to produce radicals with extended conjugation in comparable chain reactions (see supporting information).

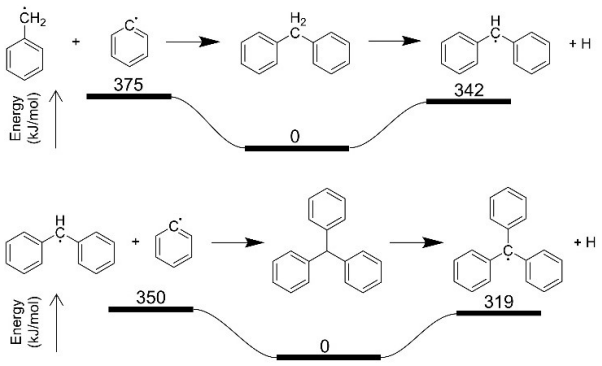

Scheme 1. The diphenylmethyl radical is formed by a well-skipping recombination of benzyl and phenyl radicals. A second phenyl addition forms triphenylmethyl by a similar well-skipping route. Both reactions are exothermic. Energy diagrams were calculated at the M06-2X / 6-311+G(3df,2p) // B3LYP / 6-311G(d,p) level of theory with zero-point corrections. The energies for the first reaction have been calculated previously[14d] and agree within 2 kJ/mol.

We used a silicon carbide tubular reactor that was resistively heated up to 1600 K at its hottest point and an electron ionization time-of-flight mass spectrometer to probe the products of this reaction as a function of temperature. Some of the flow dynamics for this type of reactor have been simulated[28] and measured[29] previously. Phenyl and benzyl radicals were produced through flash pyrolysis using nitrosobenzene and benzyl bromide as precursors, respectively. The mixture entering the reactor was 0.11% nitrosobenzene (0.05 +/- 0.02 sccm) and 0.09% benzyl bromide (0.05 +/- 0.01 sccm) in helium (50 sccm), flowing continuously. Sample mass spectra are shown in Fig. 1 for three reactor temperatures (800, 1300, and 1600 K), with insets highlighting the signal of diphenylmethane (*m/z* = 168.09; $C_{13}H_{12}$), diphenylmethyl radical (*m/z* = 167.09, $C_{13}H_{11}$), triphenylmethane (*m/z* = 244.13; $C_{19}H_{16}$), and triphenylmethyl radical (*m/z* = 243.12; $C_{19}H_{15}$).

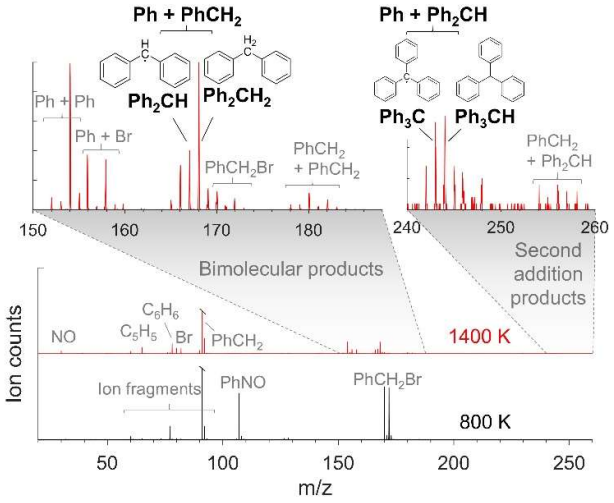

Figure 1. Electron impact mass spectra for a heated mixture of nitrosobenzene and benzyl bromide in helium. The chain reaction products diphenylmethyl radical (*m/z* 167.09) and triphenylmethyl radical (*m/z* 243.12) are visible at 1400 K.

The mass spectra indicate that at temperatures above 1100 K both the phenyl and benzyl reactants are present. Figure 2a shows a signal above 1000 K at *m/z* = 154.08 (biphenyl, $C_{12}H_{10}$), which we use here as an indicator of the presence of the phenyl radical. Phenyl could not be observed directly because the signal at *m/z* = 77.04 (phenyl, C_6H_5) is dominated by ion fragmentation from various species including nitrosobenzene. Benzyl radicals (*m/z* 91.06, C_7H_7) are observed at temperatures above 1100 K (see Fig. 2a). The high-temperature decomposition of the benzyl radical has been studied previously,[30] and a small amount of the product cyclopentadienyl radical (*m/z* 65.04, C_5H_5) is observed here (Fig. 1). Ion fragmentation of benzyl bromide contributes to the apparent C_7H_7 signal at *m/z* = 91.06, and we subtracted this contribution by assuming that at 800 K this signal is entirely due to benzyl bromide (measured independently at all temperatures at *m/z* = 169.97, 171.97) and not benzyl radicals. The energy of the ionizing electrons was kept low, 10 eV, to minimize ion fragmentation, but the electron source has a substantial spectral width that still causes some fragmentation.

Diphenylmethane (Ph_2CH_2) is observed with nearly the same temperature dependence as the benzyl radical (Fig. 2b), while the diphenylmethyl radical (Ph_2CH) is observed in the same temperature range but increases compared to Ph_2CH_2 with increasing temperature as predicted by computations.[14d] In contrast, a sample of Ph_2CH_2 showed a constant ratio between *m/z* 167.09 and *m/z* 168.09 (Fig. 2c), confirming that thermalized Ph_2CH_2 does not decompose to Ph_2CH at these temperatures but only has a constant amount of ion fragmentation contributing to *m/z* 167.09. The difference in ratio for the Ph + $PhCH_2$ reaction compared to the sample of Ph_2CH_2 indicates that the H-atom loss to form Ph_2CH is a prompt, well-skipping dissociation. All Ph_2CH_2 signals are corrected for ^{13}C contributions from *m/z* 167.09 assuming the natural abundance of ^{13}C, and Ph_2CH signals are similarly corrected whenever *m/z* 166.08 (presumed to be fluorene or 4aH-fluorene) levels are significant. Other $C_{13}H_{9\text{-}12}$ isomers are also possible from analogous chain reactions initiated at alternative Ph addition sites.

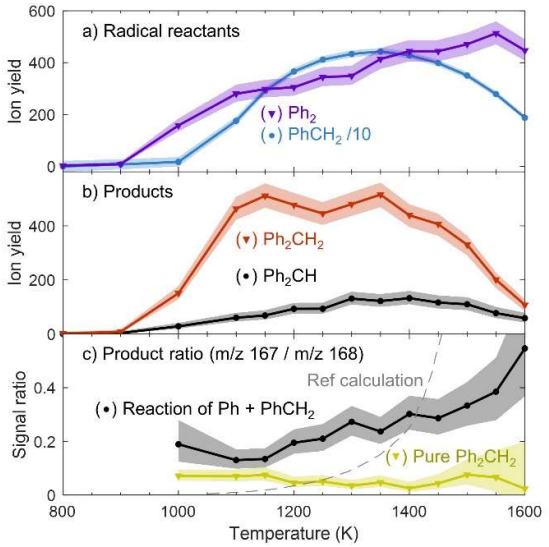

Figure 2. Temperature dependence of reactants and products. a) Both benzyl ($PhCH_2$) and phenyl (Ph) radicals are present above 1100 K. Biphenyl (Ph_2) is used to track Ph because of a large signal from ion fragmentation at the mass of Ph, *m/z* = 77.04. b) The Ph_2CH_2 (*m/z* 168.09) and Ph_2CH (*m/z* 167.09) signals resemble those of the $PhCH_2$ precursor. c) More *m/z* 167.09 signal is found compared to *m/z* 168.09 for the Ph + $PhCH_2$ reaction than a control experiment with only Ph_2CH_2, especially at higher temperatures where well-skipping reactions are more expected. The expected ratio from prior calculation[14d] is shown for comparison. Shaded regions show the Pearson 95% confidence interval for the mean of a Poisson distribution (i.e. shot noise). Multiple sources of error, where applicable, are combined in quadrature.

Theoretical product yields for the Ph + $PhCH_2$ reaction have been calculated previously by Matsugi & Miyoshi[14d] (supplementary information). According to these calculations, the H-loss channel from the Ph_2CH_2 adduct requires only 344 kJ/mol (consistent with 342 kJ/mol in Scheme 1) while the C-C cleavage to return to the reactants requires 376 kJ/mol (consistent with 375 kJ/mol in Scheme 1), yet the rate coefficient for the latter is about a factor of 3 higher across a wide temperature and pressure range due to entropic effects. Although this prediction cannot be directly compared to the experiment, as the C-C cleavage simply recovers the reactants, substantial product Ph_2CH is observed. A full model of the reactor is possible[28] but beyond the scope of this work. Absolute concentrations are not available in this study due to the difficulty of measuring the ionization cross section of the radical, but the temperature dependence of each species and the ratio of Ph_2CH to Ph_2CH_2 (Fig. 2c) can be compared to calculations. Rate coefficients are calculated at 10 Torr, while the pressure in the reactor varies from 75 Torr at the inlet to vacuum at the outlet (around 25 Torr in the hottest region). The observed ratio of Ph_2CH/Ph_2CH_2 exhibits the same trend as the well-skipping calculation predicts, increasing with temperature from 1100 K to 1600 K. In particular, the calculation predicts very low Ph_2CH_2 yield above 1500 K, causing the ratio to increase rapidly. The experiment confirms, though to a lesser extent, the rapid fall of the Ph_2CH_2 yield. The survival of more Ph_2CH_2 above 1500 K than expected is likely caused by some Ph_2CH_2 forming at a lower temperature early in the reactor and thermally stabilizing before reaching the highest temperature region (see supporting information). Depletion of the reactants, due to self-reaction or decomposition, should affect both Ph_2CH_2 and Ph_2CH equally, and while Ph_2CH can participate in further reactions (see below),

the Ph_2CH_2 is unlikely to react and cause the observed decrease at high temperatures. H abstraction from Ph_2CH_2 by Ph or $PhCH_2$ radicals could potentially produce Ph_2CH and cause the observed decrease in Ph_2CH_2. Additional results from varying the concentration of each reactant are most consistent with the well-skipping route, as Ph_2CH and Ph_2CH_2 have the same approximately first order dependence on both reactants (see supporting information). Surface reactions on the inside walls of the reactor cannot be eliminated in the small reactor used here, and these reactions allow radicals to gain H atoms to form closed-shell products. Thus, surface reactions are likely responsible for the observed benzene (m/z 78.05) and toluene (m/z 92.06) but are unlikely to produce Ph_2CH (see supporting information).

The high yield of Ph_2CH radicals (Ph + $PhCH_2$ – H) contrasts with the equivalent H loss reactions of Ph + Ph and $PhCH_2$ + $PhCH_2$, labelled in Fig. 1. Both the phenyl self-reaction[22, 31] and benzyl self-reaction[24, 32] have been studied previously, and as shown in Fig. 1 they do not produce substantial radical concentrations. In both cases, loss of one H atom from the adduct is closely followed by loss of a second (and potentially a third and fourth) H atom at the temperatures studied here, as there is no extended conjugation of the intermediate radicals. Even the small amounts of apparent radical concentration at *m/z* 153.07 and *m/z* 181.10 likely arise from H-loss *after ionization* (ion fragmentation) of the adducts due to electron ionization. Notably, the Ph_2CH radical does also show some further H loss, especially above 1400 K, to produce $C_{13}H_{10}$ (*m/z* 166.08), likely either fluorene or 4aH-fluorene (Fig. 3). These species can lose a third H atom to create a thermally stable $C_{13}H_9$ radical (*m/z* 165.07), presumed to be fluorenyl radical, observed here above 1500 K (Fig. 3) and also in the original CHRCR work.[12]

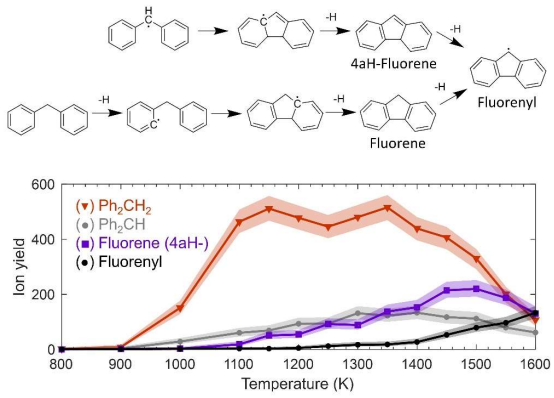

Figure 3. Fluorene and fluorenyl radicals are produced from the ring closure of Ph_2CH and Ph_2CH_2. Two likely pathways are shown, but other pathways and other isomers are possible.

The radical-radical chain reaction propagates when the radical product of the first reaction becomes a reactant in a second, similar reaction. Most of the Ph_2CH seems to be long-lived under the experimental conditions, allowing a small portion to react with phenyl radicals, limited by the abundance of phenyl radicals. This reaction can produce stable triphenylmethane (Ph_3CH) or undergo another chain reaction to produce the fully conjugated triphenylmethyl (Ph_3C) radical (Scheme 1). While the temperature dependence of the Ph_3CH yield is very similar to that of Ph_2CH (as expected for a constant Ph concentration), the Ph_3C radical yield is further shifted to higher temperatures (Fig. 4) just as Ph_2CH is shifted compared to Ph_2CH_2 (Fig. 2), consistent with well-skipping. This second phenyl addition appears to be less probable than decomposition of Ph_2CH (to fluorene and fluorenyl) under the present conditions, judging by comparing the yield of each product to that of Ph_2CH (Figs. 3&4). Note that more energetic electrons were used for ionization in the second phenyl addition experiment (12 eV for Fig 4, vs 10 eV for Fig 3). The balance between pathways likely depends on concentration, where higher phenyl concentration could enhance the efficacy of the second phenyl addition. Comparing first and second phenyl addition, the second addition may have similar or higher efficacy than the first, as the ratio of Ph_3C/Ph_2CH is higher than the ratio of $Ph_2CH/PhCH_2$. Both of these direct signal comparisons should be considered rough estimates due to the unknown ionization cross sections and discrimination factors. Trace amounts of benzyl addition to Ph_2CH are also visible (Fig. 1), but this reaction is unlikely to produce conjugated radicals. No third phenyl addition is observed here, but the Ph_3CH radical may be large enough to trigger nucleation, for example through chemisorption of smaller π-radicals.[17]

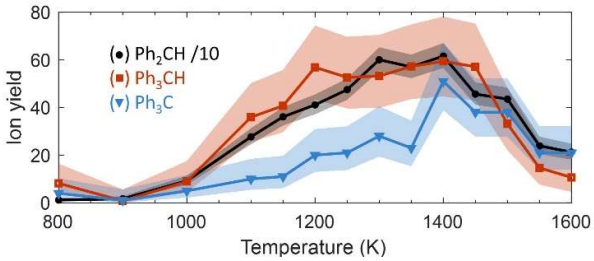

Figure 4. Evidence for the second phenyl addition and formation of triphenylmethyl (Ph_3C) radical. The temperature profiles of Ph_2CH and Ph_3CH (*m/z* 244.13) are very similar, while Ph_3C (*m/z* 243.12) increases with increasing temperature consistent with prompt H loss. More energetic electrons were used for ionization here (12 eV) in order to increase signal.

In summary, we have observed the radical-radical chain reaction of phenyl and benzyl radicals to form the Ph_2CH radical by prompt, well-skipping H-atom loss. The chain reaction continues when Ph_2CH associates with phenyl radicals to form Ph_3CH and Ph_3C. This direct observation of a radical chain reaction supports the CHRCR mechanism where radical-radical recombination is followed by rapid H loss to produce larger aliphatically bridged RSRs without decreasing the radical pool. These chain reactions could provide a fast route to larger PAH formation or nucleation in carbon-rich combustion or astrochemical environments, though further study is needed to determine the rate of chain reaction under the appropriate environmental conditions.

Experimental Details in the Supporting Information.

Acknowledgements

The authors are grateful to Jatinder Sampathkumar for assistance in designing the microreactor setup. All authors acknowledge support from the U.S. DOE, Office of Science, Office of Basic Energy Sciences, Division of Chemical Sciences, Geosciences and Biosciences. Sandia National Laboratories is a multimission laboratory managed and operated by the National Technology

and Engineering Solutions of Sandia, LLC, a wholly owned subsidiary of Honeywell International, Inc., for the U.S. DOE's National Nuclear Security Administration under contract DENA0003525. This paper describes objective technical results and analysis. Any subjective views or opinions that might be expressed in the paper do not necessarily represent the views of the U.S. DOE or the U.S. Government.

Keywords: flash pyrolysis • hydrocarbon clustering • polycycles • polycyclic aromatic hydrocarbons (PAH) • radical reactions

[1] a) U.S. EPA. Integrated Science Assessment (ISA) for Particulate Matter (Final Report, Dec 2019). U.S. Environmental Protection Agency, Washington, DC, EPA/600/R-19/188, 2019; b) H. Wang, *Proc. Combust. Inst.* **2011**, *33*, 41-67; c) J. S. Lighty, J. M. Veranth, A. F. Sarofim, *J. Air Waste Manage. Assoc.* **2000**, *50*, 1565-1618.

[2] a) J. J. Deng, Y. You, V. Sahajwalla, R. K. Joshi, *Carbon* **2016**, *96*, 105-115; b) M. U. Zahid, E. Pervaiz, A. Hussain, M. I. Shahzad, M. B. K. Niazi, *Mater. Res. Express* **2018**, *5*; c) H. Zhang, H. Zhou, Y. Wang, S. Li, P. Biswas, *Energy Fuels* **2021**, *35*, 63-85; d) S. Pokhrel, L. Mädler, *Energy Fuels* **2020**, *34*, 13209-13224.

[3] D. E. Rosner, *Ind. Eng. Chem. Res.* **2005**, *44*, 6045-6055.

[4] A. G. G. M. Tielens, *Rev. Mod. Phys.* **2013**, *85*, 1021-1081.

[5] R. I. Kaiser, N. Hansen, *J. Phys. Chem. A* **2021**, *125*, 3826-3840.

[6] a) M. Frenklach, D. W. Clary, W. C. Gardiner, S. E. Stein, *Symp. (Int.) Combust., [Proc.]* **1985**, *20*, 887-901; b) M. Frenklach, W. C. Gardiner, S. E. Stein, D. W. Clary, T. Yuan, *Combust. Sci. Technol.* **1986**, *50*, 79-115; c) M. Frenklach, H. Wang, *Symp. (Int.) Combust., [Proc.]* **1991**, *23*, 1559-1566; d) D. S. N. Parker, R. I. Kaiser, T. P. Troy, M. Ahmed, *Angew. Chem., Int. Ed.* **2014**, *53*, 7740-7744; e) T. Yang, T. P. Troy, B. Xu, O. Kostko, M. Ahmed, A. M. Mebel, R. I. Kaiser, *Angew. Chem., Int. Ed.* **2016**, *55*, 14983-14987.

[7] R. I. Kaiser, D. S. N. Parker, A. M. Mebel, in *Annual Review of Physical Chemistry, Vol 66, Vol. 66* (Eds.: M. A. Johnson, T. J. Martinez), **2015**, pp. 43-67.

[8] a) B. Shukla, A. Susa, A. Miyoshi, M. Koshi, *J. Phys. Chem. A* **2008**, *112*, 2362-2369; b) S. Xiong, J. Li, J. Wang, Z. Li, X. Li, *Comput. Theor. Chem.* **2012**, *985*, 1-7; c) L. Zhao, M. B. Prendergast, R. I. Kaiser, B. Xu, U. Ablikim, M. Ahmed, B. J. Sun, Y. L. Chen, A. H. H. Chang, R. K. Mohamed, F. R. Fischer, *Angew. Chem., Int. Ed.* **2019**, *58*, 17442-17450.

[9] N. Hansen, M. Schenk, K. Moshammer, K. Kohse-Höinghaus, *Combust. Flame* **2017**, *180*, 250-261.

[10] a) A. M. Mebel, A. Landera, R. I. Kaiser, *J. Phys. Chem. A* **2017**, *121*, 901-926; b) D. S. N. Parker, F. T. Zhang, Y. S. Kim, R. I. Kaiser, A. Landera, V. V. Kislov, A. M. Mebel, A. Tielens, *Proc. Natl. Acad. Sci. U. S. A.* **2012**, *109*, 53-58; c) A. M. Thomas, M. Lucas, T. Yang, R. I. Kaiser, L. Fuentes, D. Belisario-Lara, A. M. Mebel, *ChemPhysChem* **2017**, *18*, 1971-1976; d) L. Zhao, R. I. Kaiser, B. Xu, U. Ablikim, M. Ahmed, M. M. Evseev, E. K. Bashkirov, V. N. Azyazov, A. M. Mebel, *Angew. Chem., Int. Ed.* **2020**, *59*, 4051-4058; e) L. Zhao, R. I. Kaiser, B. Xu, U. Ablikim, M. Ahmed, M. V. Zagidullin, V. N. Azyazov, A. H. Howlader, S. F. Wnuk, A. M. Mebel, *J. Phys. Chem. Lett.* **2018**, *9*, 2620-2626; f) L. Zhao, R. I. Kaiser, B. Xu, U. Ablikim, M. Ahmed, M. M. Evseev, E. K. Bashkirov, V. N. Azyazov, A. M. Mebel, *Nat. Astron.* **2018**, *2*, 973-979; g) L. Zhao, B. Xu, U. Ablikim, W. C. Lu, M. Ahmed, M. M. Evseev, E. K. Bashkirov, V. N. Azyazov, A. H. Howlader, S. F. Wnuk, A. M. Mebel, R. I. Kaiser, *ChemPhysChem* **2019**, *20*, 791-797; h) L. Zhao, R. I. Kaiser, B. Xu, U. Ablikim, W. C. Lu, M. Ahmed, M. M. Evseev, E. K. Bashkirov, V. N. Azyazov, M. V. Zagidullin, A. N. Morozov, A. H. Howlader, S. F. Wnuk, A. M. Mebel, D. Joshi, G. Veber, F. R. Fischer, *Nat. Commun.* **2019**, *10*; i) L. Zhao, R. I. Kaiser, W. C. Lu, O. Kostko, M. Ahmed, M. M. Evseev, E. K. Bashkirov, A. D. Oleinikov, V. N. Azyazov, A. M. Mebel, A. H. Howlader, S. F. Wnuk, *Phys. Chem. Chem. Phys.* **2020**, *22*, 22493-22500; j) L. Zhao, R. I. Kaiser, W. C. Lu, M. Ahmed, M. M. Evseev, E. K. Bashkirov, V. N. Azyazov, C. Tonshoff, F. Reicherter, H. F. Bettinger, A. M. Mebel, *Angew. Chem., Int. Ed.* **2020**, *59*, 11334-11338; k) R. I. Kaiser, D. S. N. Parker, A. M. Mebel, *Annu. Rev. Phys. Chem.* **2015**, *66*, 43-67.

[11] S. Doddipatla, G. R. Galimova, H. Wei, A. M. Thomas, C. He, Z. Yang, A. N. Morozov, C. N. Shingledecker, A. M. Mebel, R. I. Kaiser, *Sci. Adv.* **2021**, *7*, eabd4044.

[12] K. O. Johansson, M. P. Head-Gordon, P. E. Schrader, K. R. Wilson, H. A. Michelsen, *Science* **2018**, *361*, 997-1000.

[13] I. Cherchneff, *Astron. Astrophys.* **2012**, *545*.

[14] a) A. N. Morozov, A. M. Mebel, *J. Phys. Chem. A* **2019**, *123*, 1720-1729; b) A. N. Morozov, A. M. Mebel, *Phys. Chem. Chem. Phys.* **2020**, *22*, 6868-6880; c) J. A. Miller, S. J. Klippenstein, *J. Phys. Chem. A* **2003**, *107*, 7783-7799; d) A. Matsugi, A. Miyoshi, *Proc. Combust. Inst.* **2013**, *34*, 269-277.

[15] M. Frenklach, A. M. Mebel, *Phys. Chem. Chem. Phys.* **2020**, *22*, 5314-5331.

[16] a) H. F. Jin, J. J. Guo, T. Y. Li, Z. Y. Zhou, H. G. Im, A. Farooq, *Fuel* **2021**, *289*; b) G. Kukkadapu, S. W. Wagnon, W. J. Pitz, N. Hansen, *Proc. Combust. Inst.* **2021**, *38*, 1477-1485.

[17] A. Menon, J. W. Martin, J. Akroyd, M. Kraft, *J. Phys. Chem. A* **2020**, *124*, 10040-10052.

[18] K. Gleason, F. Carbone, A. J. Sumner, B. D. Drollette, D. L. Plata, A. Gomez, *Combust. Flame* **2021**, *223*, 398-406.

[19] E. Wang, J. Ding, *Chem. Phys. Lett.* **2021**, *768*, 138407.

[20] a) D. W. Kohn, H. Clauberg, P. Chen, *Rev. Sci. Instrum.* **1992**, *63*, 4003-4005; b) X. Zhang, A. V. Friderichsen, S. Nandi, G. B. Ellison, D. E. David, J. T. McKinnon, T. G. Lindeman, D. C. Dayton, M. R. Nimlos, *Rev. Sci. Instrum.* **2003**, *74*, 3077-3086.

[21] K. H. Fischer, J. Herterich, I. Fischer, S. Jaeqx, A. M. Rijs, *J. Phys. Chem. A* **2012**, *116*, 8515-8522.

[22] P. Constantinidis, H. C. Schmitt, I. Fischer, B. Yan, A. M. Rijs, *Phys. Chem. Chem. Phys.* **2015**, *17*, 29064-29071.

[23] P. Constantinidis, F. Hirsch, I. Fischer, A. Dey, A. M. Rijs, *J. Phys. Chem. A* **2017**, *121*, 181-191.

[24] F. Hirsch, P. Constantinidis, I. Fischer, S. Bakels, A. M. Rijs, *Chem. - Eur. J.* **2018**, *24*, 7647-7652.

[25] L. Zhao, W. Lu, M. Ahmed, M. V. Zagidullin, V. N. Azyazov, A. N. Morozov, A. M. Mebel, R. I. Kaiser, *Sci. Adv.* **2021**, *7*, eabf0360.

[26] L. Zhao, R. I. Kaiser, W. C. Lu, B. Xu, M. Ahmed, A. N. Morozov, A. M. Mebel, A. H. Howlader, S. F. Wnuk, *Nat. Commun.* **2019**, *10*.

[27] M. Hausmann, P. Hebgen, K.-H. Homann, *Symp. (Int.) Combust., [Proc.]* **1992**, *24*, 793-801.

[28] Q. Guan, K. N. Urness, T. K. Ormond, D. E. David, G. Barney Ellison, J. W. Daily, *Int. Rev. Phys. Chem.* **2014**, *33*, 447-487.

[29] R. S. Tranter, A. L. Kastengren, J. P. Porterfield, J. B. Randazzo, J. P. A. Lockhart, J. H. Baraban, G. B. Ellison, *Proc. Combust. Inst.* **2017**, *36*, 4603-4610.

[30] a) G. T. Buckingham, T. K. Ormond, J. P. Porterfield, P. Hemberger, O. Kostko, M. Ahmed, D. J. Robichaud, M. R. Nimlos, J. W. Daily, G. B. Ellison, *J. Chem. Phys.* **2015**, *142*, 044307; b) G. T. Buckingham, J. P. Porterfield, O. Kostko, T. P. Troy, M. Ahmed, D. J. Robichaud, M. R. Nimlos, J. W. Daily, G. B. Ellison, *J. Chem. Phys.* **2016**, *145*, 014305; c) A. Matsugi, *J. Phys. Chem. A* **2020**, *124*, 824-835.

[31] R. S. Tranter, S. J. Klippenstein, L. B. Harding, B. R. Giri, X. Yang, J. H. Kiefer, *J. Phys. Chem. A* **2010**, *114*, 8240-8261.

[32] S. Sinha, A. Raj, *Phys. Chem. Chem. Phys.* **2016**, *18*, 8120-8131.

Entry for the Table of Contents

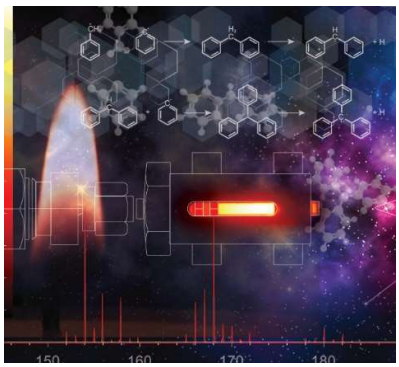

Radical-radical chain reactions may contribute to rapid growth of polycyclic aromatic hydrocarbons in combustion and astrochemical environments. Phenyl and benzyl radicals are experimentally observed to complete this chain reaction, producing diphenylmethyl and triphenylmethyl radicals by prompt H-atom loss. This observation confirms the plausibility of such chain reactions at high temperature and low pressure.

Institute Twitter username: @SandiaLabs (Sandia National Labs)

Supporting Information

Experimental observation of hydrocarbon growth by resonance stabilized radical-radical chain reaction

David E. Couch, Angie J. Zhang, Craig A. Taatjes, Nils Hansen*

Abstract: Rapid molecular weight growth of hydrocarbons has been observed in flames, implied in cold astrochemical environments, and harnessed in industrial synthesis. A variety of high- and low-temperature chemical mechanisms have been proposed and confirmed, but more facile pathways may be needed to explain observations. We provide laboratory confirmation in a controlled pyrolysis environment of a recently proposed mechanism, radical-radical chain reactions of resonance-stabilized species. The recombination reaction of phenyl (c-C_6H_5) and benzyl (c-$C_6H_5CH_2$) radicals produces both diphenylmethane and diphenylmethyl radicals, the latter increasing with rising temperature. A second phenyl addition to the product radical forms both triphenylmethane and triphenylmethyl radicals, confirming the propagation of radical-radical chain reactions under the experimental conditions of high temperature (1100-1600 K) and low pressure (~3 kPa). Similar chain reactions may contribute to particle nucleation in flames and the interstellar medium and could occur in industrial particle growth.

DOI: 10.1002/anie.202110929

Table of Contents

Experimental Procedures

Helium with approximately 0.1% (by volume) nitrosobenzene (PhNO) and benzyl bromide ($PhCH_2Br$) flows through a heated microreactor into a high vacuum chamber. The gas jet is sampled by electron impact ionization coupled with time-of-flight mass spectrometry.

Helium (Matheson) flows at 50 sccm through a mass flow controller (MKS 647C), then splits to run through parallel bubblers as well as a bypass. One bubbler contains solid, powdered nitrosobenzene (≥97%, Sigma-Aldrich), and the other contains liquid benzyl bromide (98%, Sigma-Aldrich), each held in a 0.5 mL glass vial (Pyrex Vista), with the helium flowing through the head space rather than actually bubbling through the sample. The concentration of nitrosobenzene in the stream was found by weighing the sample vial before and after a set of experiments that lasted several hours with constant flow conditions, assuming the rate of evaporation was constant during this time. The concentration of benzyl bromide was measured more accurately by measuring the height of liquid sample in the vial approximately every 15 minutes during the entire set of experiments, and the evaporation rate was nearly constant over the whole duration. For the results shown in the main text, the evaporation rate for nitrosobenzene was 0.054 ± 0.020 sccm and for benzyl bromide 0.046 ± 0.007 sccm, yielding relative concentrations of 0.11% and 0.09% respectively.

The gas mixture flows continuously through a resistively heated silicon carbide tube described previously.[1] The tube is 28 mm long, ID 1 mm, heated up to 1600 K at the hottest point. Electric current flows through the silicon carbide between two graphite electrodes that contact molybdenum clips held in place by an alumina heat shield (Fig. S1). The heat shield, molybdenum clips, graphite disks, and silicon carbide tubes were obtained from the CIRES instrument shop at the University of Colorado Boulder (tubes originate from Saint Gobain but are treated in the instrument shop). The exit of the reactor serves as a choke point, causing a supersonic expansion of the gas into the vacuum chamber. The supersonic gas jet is sampled by a 0.4 mm skimmer (Beam Dynamics). The pressure in the source chamber reaches about $2x10^{-4}$ Torr during operation, while the pressure behind the skimmer is kept below 10^{-6} Torr.

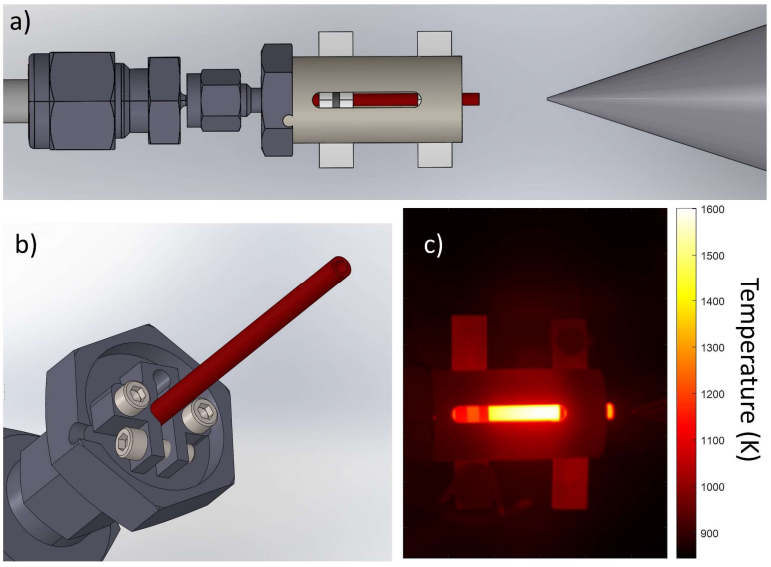

Figure S1. a) The supersonic jet exits the hot microreactor to be sampled by a skimmer. The reactor (red) is resistively heated by passing DC current between the molybdenum electrodes (light grey). b) The reactor is held in place by a clamp with symmetric bolts to prevent tipping. c) An open slot in the heat shield permits optical access for thermal measurement. An observed thermal image is shown.

A slot was cut in the heat shield to allow an optical pyrometer (Micro-Epsilon TIM M-1) to measure the reactor temperature. A thermal image of the reactor during an experiment is shown in Fig. S1c. The emissivity of silicon carbide was assumed to be 0.82 based on published measurements.[2] The temperature of the silicon carbide should be measured correctly to within 2%, while the surrounding materials scatter light emitted from the hot tube and are not measured correctly.

The flow properties of these tubular reactors, including temperature, velocity, and pressure profiles of the centerline, have been simulated previously.[3] The pressure profile and interior geometry were measured previously using xenon x-ray fluorescence.[4] We estimate that the pressure at the hottest point of the reactor is about 1/3 that of the inlet pressure, so around 25 Torr at 1600 K. Observed inlet pressures are shown in Table S1. The inlet pressure increases with increasing temperature due to expansion of the gas within the reactor and increasing viscosity of helium. The electrical current and voltage necessary to maintain each temperature are also given. The resistivity of silicon carbide decreases with increasing temperature such that the voltage remains nearly constant while higher current is needed to reach higher temperatures. A previously heated tube requires about 50 V at 300 K to begin heating, while a fresh tube requires a much higher voltage depending on its treatment.

Table S1. Electrical and pressure measurements of the reactor, with 50 sccm flow of mostly helium as described above.

Temperature (K)[a]	Current (A)[b]	Voltage (V)[b]	Pressure (Torr)[c]
300	0	0	25.5
800	1.02	7.6	50.1
900	1.58	7.8	52.6
1000	2.02	7.6	55.8
1100	2.47	7.8	59.0
1150	2.69	7.7	61.2
1200	2.94	7.8	63.1
1250	3.17	7.9	64.6
1300	3.43	8.1	65.9
1350	3.68	8.2	67.0
1400	3.94	8.4	68.4
1450	4.20	8.6	70.0
1500	4.46	8.8	71.4
1550	4.73	9.0	72.9
1600	5.04	9.3	74.5

[a] Highest temperature observed on the reactor. [b] Current and voltage (DC) supplied to the reactor. [c] Pressure measured between the flow controller and the bubblers.

The gas jet passing through the skimmer is sampled by electron impact ionization to a time-of-flight mass spectrometer (Kaesdorf). The peak of the electron energy distribution can be quickly changed, but a small flux of high energy electrons is always present. This high energy tail causes some ion fragmentation. Ions are sampled at a rate of 30 kHz and pass through a Reflectron mass spectrometer to a microchannel plate (Photonis Long-Life^{TM} 40mm). We observe mass resolution of $m/\Delta m \approx 2700$, sufficient to resolve $C_7H_7{}^{79}Br$ from $C_{13}H_{14}$ and similarly for other bromides.

Possible role of isomers

The first and second phenyl addition can occur at more than one site, creating the possibility of several isomers. For the first phenyl addition to the benzyl radical, the addition is most likely to occur at the CH_2 site, but the radical is delocalized with some component at the *ortho* and *para* sites. Figure S2 shows that each of the three likely phenyl addition reactions produces a closed-shell adduct with an sp^3-hybridized carbon, while the loss of an H atom at the addition site produces a fully-conjugated radical. Thus, the chain reaction is likely to propagate in any of these configurations. In the present experiment, isomers are not distinguished, so all of these channels may be operating in parallel. Each of the three radicals produced from the first phenyl addition have multiple sites for a second phenyl addition, and once again the loss of an H atom from the sp^3-hybridized carbon returns the full conjugation. The three likely pathways for addition to Ph_2CH are shown in Fig. S2.

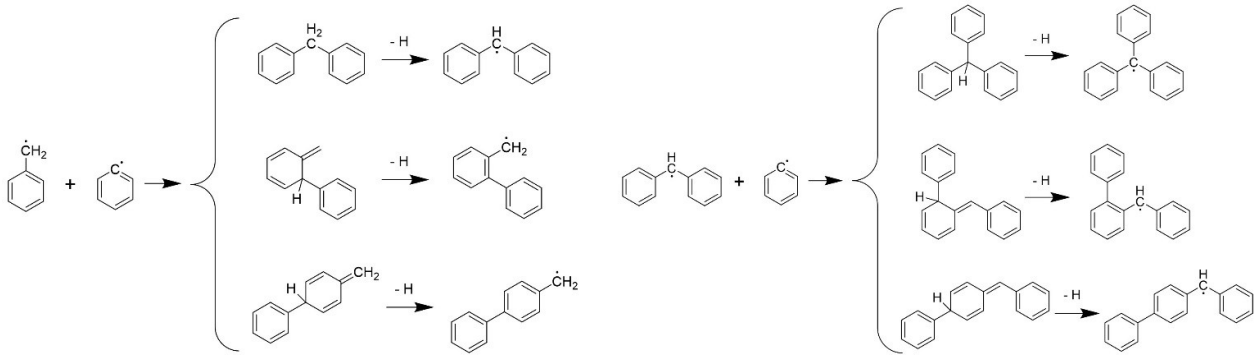

Figure S2. The $PhCH_2$ + Ph reaction can produce three different isomers of $C_{13}H_{12}$, each of which can promptly lose an H atom to produce a conjugated radical. Each of these radicals has multiple sites for a second phenyl addition. The chain reaction pathways for production of $C_{19}H_{16}$ and $C_{19}H_{15}$ are shown only for second phenyl addition to the Ph_2CH radical.

Surface reactions

Previous unpublished work using these silicon carbide reactors has found that many radicals can abstract H atoms from the inside walls of the reactor. This is most likely due to soot building up on the walls. From previous measurements, we estimate that the amount of H abstraction product is typically around 10-30% of the radical concentration, but sometimes the abstraction product persists at higher temperatures than the radical. In this work, the most important abstraction reaction would be Ph_2CH abstracting H to form Ph_2CH_2. We note that this reaction would have the opposite effect from that observed in this work, where the Ph_2CH_2 decreases faster at high temperature. Thus, we do not think surface reactions affect the main conclusion of this paper, that Ph_2CH is produced by a well-skipping route, but surface reactions could perhaps contribute to the discrepancy between theory and experiment in Figure 2. We observe two other wall reactions: phenyl producing benzene, and benzyl producing toluene. These reactions may deplete the phenyl and benzyl concentrations, but the products should not interfere with the reactions of interest. Below, we confirm that the primary source of toluene ($PhCH_3$) is not H abstraction of benzyl ($PhCH_2$) from Ph_2CH_2, a reaction that would have complicated the present experiment.

Concentration dependence of diphenylmethyl radical

While the diphenylmethane (Ph_2CH_2) is almost certainly a direct product of the Ph + $PhCH_2$ reaction, the origin of the diphenylmethyl radical (Ph_2CH) is less certain. We assert in this paper that the radical arises from a prompt H-loss caused by the excess vibrational energy of Ph_2CH_2. This seems likely both because the products Ph_2CH and H have a lower total enthalpy of formation than the reactants Ph and $PhCH_2$, and because the calculations of Matsugi and Miyoshi[5] indicate that this prompt H loss should be a substantial pathway. However, another valid explanation is that a second phenyl or benzyl radical abstracts the H atom from Ph_2CH_2 to yield Ph_2CH. H abstraction likely has a barrier that is significant at these temperatures, but we not have investigated these barriers in this work. Instead, we use concentration dependence to indicate that no second phenyl or benzyl radical is needed for Ph_2CH formation.

We performed additional experiments to measure the effect of phenyl and benzyl concentration on Ph_2CH yield. Figure S3 shows a comparison of various species to expected behavior for 0th, 1st, and 2nd order dependence on each reactant. The x-axis ion signals are the sum of signals corresponding to (a) nitrosobenzene (*m/z* 30, 77, 107) and (b) benzyl bromide (*m/z* 170, 172) using two different election energy settings (12 eV and 17 eV). Each species shown is normalized by the mean, which allows ideal 0th, 1st, and 2nd order yields to be calculated (flat, proportional, and quadratic). Only results using 17 eV electrons are shown, and this increases the chance that a mass peak has been misidentified due to ion fragmentation. Results using 12 eV electrons show similar trends but are too noisy to match to the ideal curves. The total helium flow remains at 50 sccm but the amount directed through the bubblers is varied to change the evaporation rate of each precursor. For varying nitrosobenzene, HBr, Ph_2CH_2, and Ph_2 serve as confirmation of the expected 0th, 1st, and 2nd order behavior, respectively. HBr arises from Br (a coproduct of $PhCH_2$ from benzyl bromide decomposition) abstracting H from the walls of the reactor. The HBr bond strength is quite low, so Br is unlikely to abstract from the species of interest. $PhCH_3$ (toluene) also matches 0th order, because $PhCH_2$ radicals also abstract H from the reactor walls. The ratio of $PhCH_3$ to $PhCH_2$ (not shown) remains around ¼ throughout the experiment. Ph_2CH matches 1st order in close agreement with Ph_2CH_2, indicating only one phenyl radical is necessary to make each product. For varying benzyl bromide, Ph_2 should be 0th order but drops at high benzyl bromide concentration due to an accidental drop in helium flow through the nitrosobenzene. This decrease can also be seen in both Ph_2CH and Ph_2CH_2. $PhCH_2$ and Br_2 show approximately the expected 1st and 2nd order behavior. Ph_2CH matches Ph_2CH_2, and both are most consistent with 1st order. The similarity between Ph_2CH and Ph_2CH_2 in both plots is also a good indication that Ph_2CH does not primarily form from H abstraction by phenyl or benzyl radicals, in addition to the approximately 1st order behavior in both reactants.

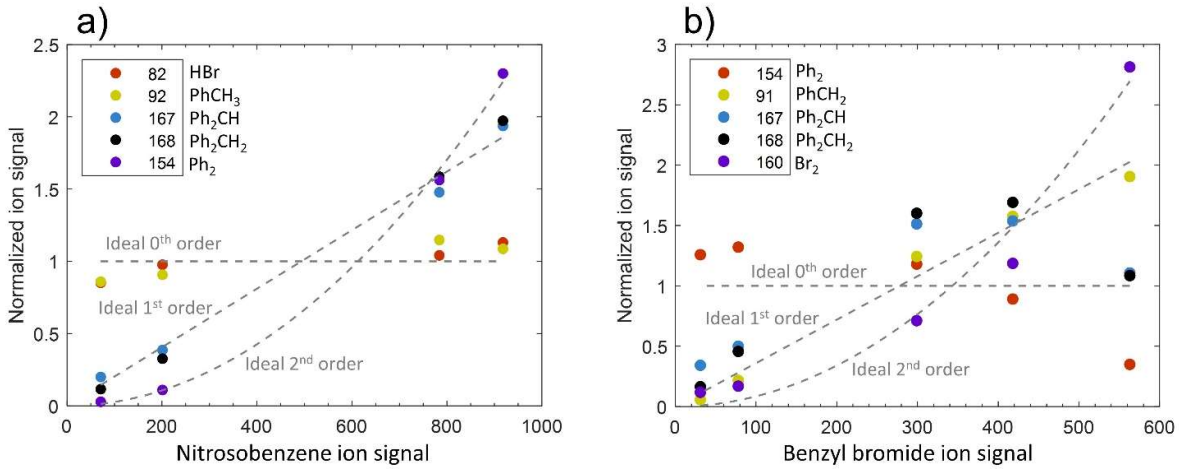

Figure S3. Comparison of (a) phenyl and (b) benzyl concentration dependence of Ph_2CH with other known products. The x-axis ion signals are the sum of signals corresponding to (a) nitrosobenzene (*m/z* 30, 77, 107) and (b) benzyl bromide (*m/z* 170, 172). Each species shown is normalized by the mean, which allows ideal 0th, 1st, and 2nd order yields to be calculated (flat, proportional, and quadratic). In (a), HBr, Ph_2CH_2, and Ph_2 serve as confirmation of the expected 0th, 1st, and 2nd order behavior, respectively. $PhCH_3$ matches 0th order, and Ph_2CH matches 1st order in close agreement with Ph_2CH_2. In (b), Ph_2 should be 0th order but drops at high benzyl bromide concentration, an effect also seen in both Ph_2CH and Ph_2CH_2. $PhCH_2$ and Br_2 show approximately the expected 1st and 2nd order behavior. Ph_2CH matches Ph_2CH_2, and both are most consistent with 1st order.

References

[1] X. Zhang, A. V. Friderichsen, S. Nandi, G. B. Ellison, D. E. David, J. T. McKinnon, T. G. Lindeman, D. C. Dayton, M. R. Nimlos, *Rev. Sci. Instrum.* **2003**, *74*, 3077-3086.

[2] L. Biasetto, M. Manzolaro, A. Andrighetto, *The European Physical Journal A* **2008**, *38*, 167-171.

[3] Q. Guan, K. N. Urness, T. K. Ormond, D. E. David, G. Barney Ellison, J. W. Daily, *Int. Rev. Phys. Chem.* **2014**, *33*, 447-487.

[4] R. S. Tranter, A. L. Kastengren, J. P. Porterfield, J. B. Randazzo, J. P. A. Lockhart, J. H. Baraban, G. B. Ellison, *Proc. Combust. Inst.* **2017**, *36*, 4603-4610.

[5] A. Matsugi, A. Miyoshi, *Proc. Combust. Inst.* **2013**, *34*, 269-277.

Author Contributions

D.E.C., C.A.T., and N.H. planned the experiment, C.A.T. and N.H. secured funding, D.E.C. and A.J.Z. designed and assembled new components and performed experiments, D.E.C. analyzed data, D.E.C. and N.H. wrote drafts, C.A.T. and N.H. directed the research.